Ozonolysis of Fluoroethene: Theoretical Study of Unimolecular Decomposition Paths of Primary and Secondary Fluorozonide

Ivan Ljubić* and Aleksandar Sabljić†

Department of Physical Chemistry, Ruđer Bošković Institute, P.O. Box 180, HR-10002, Zagreb, Republic of Croatia

Received: November 19, 2004; In Final Form: January 20, 2005

A theoretical investigation into unimolecular decomposition paths of primary (**POZF**) and secondary (**SOZF**) fluorozonide was carried out by utilizing the multiconfigurational CASSCF/cc-pVTZ level in optimizations of the stationary points and calculations of the harmonic vibrational frequencies. The dynamical electron correlation was accounted for via the multireference CASPT2/cc-pVTZ treatment based on the zeroth-order CASSCF/cc-pVTZ reference. The CASPT2 was substituted with the CCSD(T)/6-311G(2d,2p) correction whenever the former resulted in negative activation barriers. The most favorable decomposition route of **POZF** is a concerted cleavage to carbonyl oxide (CO) and formyl fluoride (FF) with fragments in the anti conformation, with regard to the orientation of the terminal oxygen in the carbonyl oxide and the flourine atom of the carbonyl compound. The ratio of unimolecular rate constants calculated within the RRKM formalism suggests that the CO−FF channel of cleavage amounts to 98%, which agrees well with the upper bound of experimental esimates. The **SOZF** decomposition most readily takes place in a stepwise manner initiated by the O−O bond rupture. Two conformational minima are exhibited by **SOZF**, the O−O and H_2C−O half-chairs. The calculated rotational constants and scaled frequencies for the O−O half-chair are in good agreement with the experimental values.

Introduction

Ozone, together with the hydroxyl and nitrate radical, belongs to the most important reactive species in the troposphere, which are capable of rapidly oxidizing and consuming many anthropogenic pollutants.[1,2] For this reason, investigations into reactivity toward ozone play a major role in assessing the overall tropospheric persistance of pollutants and ipso facto their impact on the global environment.[3] It is normally desirable that the pollutants be consumed by the reactive species in the troposphere before reaching the upper atmospheric layers, where, photochemically fragmented, they can participate in the depletion of the stratospheric ozone, as nowadays do the notorious Freons. Examples of pollutants of special concern are provided by simple halogented ethenes such as fluoroethene and chloroethene because of their widespread use as solvents, refrigerants, and in the technology of polymers[4] (e.g. fluoroethene is listed as a high production volume chemical by the Environmental Protection Agency (EPA), with annual production exceeding 4.5×10^5 kg[5]). Another dangerous facet of fluoeoethene is furnished by studies into its carcinogenicity, which anticipated it to be a human carcinogen, because there is firm evidence that its metabolites form covalent DNA adducts.[6]

Apart from representing the reactions of pronounced atmospheric interest, additions of ozone to unsaturated carbon bonds have long found their important use in preparative organic chemistry.[7] Thus, unlike saturated centers in the molecule, which are almost never attacked upon the addition of ozone, double and triple C−C bonds commonly undergo rupture (ozonolysis), whereby in the condensed phase carbonyl fragments emerge.[8]

SCHEME 1: Initial Steps in the Ozonolysis of Alkenes

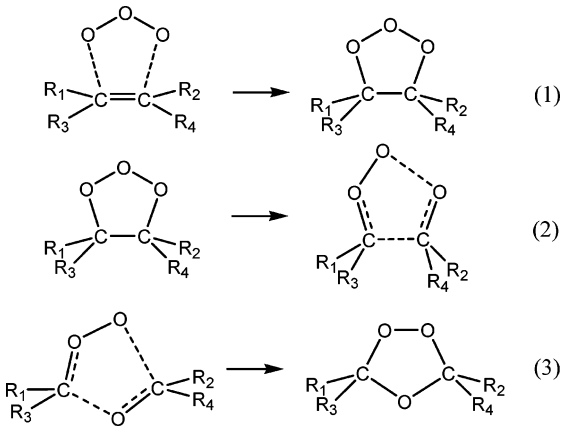

Criegee[9] postulated the succession of three [2 + 3] cycloadditions or cycloreversions involving primary ozonides (1,2,3-trioxolanes, Scheme 1(1)) and aldehyde or ketone oxides as decisive intermediates (Scheme 1(2)), resulting finally in secondary ozonides (1,2,4-trioxolanes, Scheme 1(3)).

In light of the great practical importance of ozonolyses of simple alkenes, the abundance of experimental efforts in elucidating their kinetics and detailed mechanisms is not surprising.[1,2] The most numerous are those dealing with the ozonolysis of ethene, with particular emphasis on the product yields from various reaction channels.[10] It was observed, however, that even with the simplest of halogenated alkenes a reliable experimental deduction of the mechanism and kinetics is largely complicated by the secondary reactions.[1] Some of the consequences include substantial uncertainty in yields and difficulties in achieving reproducibility.

* To whom correspondence should be addressed. E-mail: iljubic@irb.hr.
† E-mail: sabljic@irb.hr.

10.1021/jp044706h CCC: $30.25
Published on Web 02/22/2005

Mazur et al.[11] identified a number of products in the ozonolysis of fluoroethene conducted at low temperatures, either neat or in CH_3Cl. The dominant volatile products included formyl fluoride and secondary fluorozonide (3-fluoro-1,2,4-trioxolane), with minute amounts of cross secondary ozonides, acetyl fluoride, fluoroacetyl fluoride, and *cis*-1,2-difluorooxirane. The authors concluded that a major reaction pathway in fluoroethene ozonolysis is a Criegee cleavage of the primary fluorozonide (4-fluoro-1,2,3-trioxolane) to aldehyde and carbonyl oxide and that both possible pathways may occur: (a) cleavage to H_2COO and HFCO and (b) cleavage to H_2CO and HFCOO. In dominantly following the Criegee pathways (i.e., the possibility of isolating sizable quantities of the secondary ozonide), the ozonolysis of fluoroethene appeared more similar to the ozonolysis of ethene or alkylated alkenes rather than to that of other halogenated alkenes. Thus, no trace of fluoroepoxide was observed, which contrasts the sizable epoxide formation in di-, tri- and tetrafluoroethene ozonlyses.[12] The isotope labelings yielded other valuable clues as to the reaction mechanism.[13] The results suggested that routes to the secondary ozonide of fluoroethene are consistent with a Criegee cleavage, predominantly toward the H_2COO and HFCO fragments, although some production of HFCOO and H_2CO occurs as well.

As for the theoretical studies, those dealing with the ozonolysis of ethene are again by far the most numerous.[14] They all indicate a rich and intricate reaction mechanism with some queries still unresolved. In particular, the role of the intermediate carbonyl oxide is not entirely understood; suffice it to say that this species has to be postulated in the reaction mechanism because it has still not been unambiguously observed in connection to the ethene ozonolysis.[15] It is clear that an asymmetric single fluorine substitution on ethene makes the mechanism of ozonolysis even richer and more complex. Despite such a challenge, until recently there existed only a single theoretical account of the initial step of the fluoroethene ozonolysis at the RHF-MP2/6-31G* level conducted by Cremer in the early 1980s.[16] In our recent paper,[17] a complete account of the initial 1,3-bipolar addition of ozone to ethene, fluoroethene, and chloroethene was given, which is the step whose barrier solely determines the kinetic parameters comparable to the experimental values. Valuable insight into the mechanism and kinetics of the ozonolyses was obtained by utilizing the multiconfiguration complete active space self-consistent field (CASSCF) method[18] followed by the multireference-based perturbation correction up to the second order (CASPT2).[19] Throughout the reaction path, the two methods provide a simultaneous good description of both nondynamic and dynamic electron correlation, whose balance is vital for any quantitative assessment of the ozone properties[20] and naturally any reactions involving it. The CASPT2 method alone proved to be an excellent alternative to standard single-reference-based treatments in describing the force field of ozone,[21] and the performance of the CASSCF/CASPT2 approach was shown to be comparable to that of CCSD(T) in the unimolecular decomposition of the carbonyl oxide.[22] In the present paper, we continue a detailed description of the mechanism of the ozonolysis of fluoroethene in the same spirit.

A recent detailed description of the mechanism and kinetics of ethene ozonolysis by Anglada et al.[23] proved to be a valuable guide in revealing the mechanism of fluoroethene ozonolysis as well. However, a single halogen substitution contributes significantly to the complexity of the reaction because many more decomposition pathways need be considered now with regard to the important new factor, the position of the fluorine atom in the stationary structures. Upon the cleaving of the primary fluorozonide, the fluorine atom can reside either on the aldehyde or carbonyl oxide moiety. Henceforth, this basic configurational bifurcation will be designated as an a- or b-type mechanism, respectively (Scheme 2). In addition to that, the most stable conformations as to the position of the fluorine atom with regard to the terminal oxygen of the carbonyl oxide moiety (syn or anti) need be determined in a more accurate assessment of the reaction energetics.

SCHEME 2: Configurational (a and b) Types and Conformational (syn and anti) Types of Cleavage of the Primary Fluorozonide

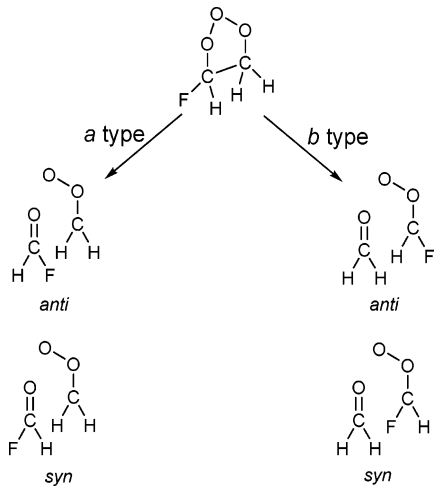

Theoretical Calculations

All stationary points on the potential energy surface were optimized at the CASSCF/cc-pVTZ level of theory, and the harmonic vibrational wavenumbers used for the zero-point vibrational energies (ZPVEs) evaluation were calculated subsequently at the same level. The cc-pVTZ is the standard Dunning's correlation consistent basis set,[24] contracted to (4s3p2d1f) on the first-row atoms and to (3s2p1d) on hydrogen. The dynamical electron correlation was accounted for at the CASPT2/cc-pVTZ level, taking the stationary CASSCF/cc-pVTZ wave functions as the zeroth-order references. The CASPT2 method is formulated as a perturbation expansion up to the second order with excitations from the CASSCF reference employing the full (i.e., nonblock diagonal) Fock matrix.[19] Because the cc-pVTZ basis set was not designed to treat the core−valence correlation, the CASPT2 energies were calculated with the core shells (1s shells on the O, C, and F atoms) kept frozen. The (10,9) active space was used, which stands for all of the spin- and symmetry-allowed distributions of 10 active electrons among 9 active orbitals. Thus, the space of configuration state functions of dimension 5292 is spanned, which turned out to be quite feasible computationally. Because we originally intended to calculate the whole of the reaction energetics by exclusively applying the CASSCF/CASPT2 multireference treatment, the (10,9) active space was kept throughout, which made the reaction profile a direct sequel of the one derived previously.[17] This size of the active space takes proper account of the most important near-degeneracy effects already in the transition state structure prior to the formation of the primary fluorozonide,[17] with respect to the criterion of active occupancies in the range of 0.02−1.98 put forward by Anglada and Bofill.[25] An inspection of the active orbital occupancies of each stationary point on the potential energy

surface showed that in no instance did there arise the need for an extension of the (10,9) active space. In calculating the reaction channels, which included the fragmentation of the nine-atom parent species, the (10,9) active space was split as follows: (1) (8,7) and (2,2) between (fluoro)carbonyl oxide and formaldehyde (formyl fluoride), (2) (6,5) and (4,4) between fluoroxirane and singlet oxygen ($^1\Delta_g$), and (3) (8,7) and (2,2) between fluorodioxirane and formaldehyde. The consistency of all active spaces was always checked by ensuring that unambiguous one-to-one correspondence could be established between the active orbitals of the adjacent stationary structures. Nevertheless, in certain cases the CASPT2 correction was found to overestimate the stabilization energies of some transition states to the extent of placing them below those of the preceding minima. The relative energies were then recalculated using the coupled-cluster approach with perturbative evaluation of the triple excitations (CCSD(T)[26]) based on the RHF reference functions. In these calculations, the standard 6-311G(2d,2p) basis set was employed, which is contracted to (4s3p2d) on O, C, and F and to (3s,2p) on H.[27] In connection to the coupled-cluster calculations, the T_1 diagnostic of Lee and Taylor[28] was calculated to estimate the importance of near-degeneracy effects by considering the norm of the single-excitation amplitudes. All multireference-based and coupled-cluster electronic structure calculations were performed with the MOLCAS version 5.4 program package.[29]

The rate constants for the unimolecular decomposition channels of the primary fluorozonide were calculated within the RRKM formalism.[30] In these calculations we adopted the rotational constants and harmonic vibrational frequencies of the more stable conformation of the reactant, which is the oxygen envelope (designated syn in ref 17). The energy distribution function $f^{\mathbf{POZF}}(E)$ of a chemically activated species is derived on the basis of an RRKM consideration of the step that involves its formation:[31]

$$f^{\mathbf{POZF}}(E) = \frac{W_{\mathrm{TSF}}(E - E_0)\exp[-(E - E_0)/k_{\mathrm{B}}T]}{\int_0^\infty W_{\mathrm{TSF}}(\epsilon)\exp[-\epsilon/k_{\mathrm{B}}T]\,\mathrm{d}\epsilon} \quad (1)$$

where $E \geq E_0$. In eq 1, W_{TSF} stands for the sum of states of the (more stable) transition-state structure $\mathbf{TSF}_{\mathrm{anti}}$ of the ozone addition to fluoroethene, and E_0 is the barrier (= 246.4 kJ mol^{-1})[17] for the reverse process starting from the primary fluorozonide. At a fixed temperature and pressure, the average rate constant $\langle k_i \rangle$ for the ith decomposition channel can be calculated within the strong-collision hypothesis according to

$$\langle k_i \rangle = \omega \frac{\int_{E_0}^\infty \{k_i(E)/[k_i(E) + \omega]\} f^{\mathbf{POZF}}(E)\,\mathrm{d}E}{\int_{E_0}^\infty \{\omega/[k_i(E) + \omega]\} f^{\mathbf{POZF}}(E)\,\mathrm{d}E} \quad (2)$$

Here, the symbol ω denotes the collision frequency, which depends on the temperature T and total pressure P according to

$$\omega = P\frac{\sigma_{\mathrm{d}}^2 N_{\mathrm{A}}}{R}\sqrt{\frac{8\pi N_{\mathrm{A}} k_{\mathrm{B}}}{\mu T}} \quad (3)$$

where σ_{d} is the collision diametar of the primary fluorozonide approximated by 3.0×10^{-10} m. The k_i microconstants are given by the classical RRKM expression

$$k_i(E) = \frac{W_{\mathrm{TS}i}(E - E_i^{\ddagger})}{hN_{\mathbf{POZF}}(E)} \quad (4)$$

where $W_{\mathrm{TS}i}$ is the sum of states including the active degrees of freedom of the transition-state structure of the ith unimolecular decomposition channel and $E_i^{\ddagger}$ is the corresponding activation barrier. The symbol $N_{\mathbf{POZF}}$ stands for the density of states of the primary fluorozonide, and h is Planck's constant. The sums and densities of the rovibrational states were determined by the standard Beyer−Swinehart counting procedure.[32] All of the vibrational degrees of freedom, which also include the trioxolane ring-puckering modes and the torsions around the single C−C bond within the stepwise manner of decomposition (vide infra), were modeled as harmonic oscillators. In some cases, the centrifugal effects, which originate from the overall rotational (adiabatic) degrees of freedom, are capable of markedly facilitating bond fissions.[31] A good estimate of these effects is provided by modifying the energy at which the k_i's are calculated by the amount $\langle \Delta E_J \rangle$

$$k_i(E + \langle \Delta E_J \rangle) = \frac{W_{\mathrm{TS}i}(E - E_i^{\ddagger})}{hN_{\mathbf{POZF}}(E + \langle \Delta E_J \rangle)} \quad (5)$$

where $\langle \Delta E_J \rangle = (1 - (I^{\ddagger}/I))k_{\mathrm{B}}T$ is the mean difference in the rotational energy of the transition state and the reactant. Here, the most interesting principal moments of inertia I are those that change significantly on going from the reactant to the transition-state structure. Because usually $I^{\ddagger} > I$ and $\langle \Delta E_J \rangle < 0$ in the course of bond fissions, adiabatic rotations release energy into the active degrees of freedom and may thus contribute to a nonnegligible increase in the unimolecular rate constant.

Results and Discussion

The CASSCF/cc-pVTZ optimized structures of minima and transition states from the concerted and stepwise decomposition of the primary fluorozonide (**POZF**) are given in Figure 1. The corresponding potential energy profiles for the two manners of configurational cleavage of **POZF** are given in Figure 2. The reaction profiles are given in terms of the relative electronic energies corrected for the diferences in ZPVEs. For a majority of the relative energies, the profile is based on the CASPT2/cc-pVTZ corrections, taking the CASSCF(10,9)/cc-pVTZ stationary functions as the zeroth order. The relative energies do not add up exactly, however, because the underlined energies (Figure 2) were calculated by a different approach at the CCSD(T)/6-311G(2d,2p) level. This was done whenever the CASPT2 correction lowered the corresponding reaction barriers to the extent that they became negative. For a discussion on these occurrences, please see section E (CCSD(T) versus CASPT2 corrections) below.

We distinguish the two basic manners of configurational cleavage of **POZF**: the first leading to the formation of carbonyl oxide and formyl fluoride (a-type mechanism) and the second to fluorocarbonyl oxide and formaldehyde (b-type mechanism). Furthermore, on the CASSCF/cc-pVTZ potential energy surface it was possible to find two conformations of each optimized structure. These conformations can be defined with respect to the δ(F−C3−C4−O1) dihedral angle in the a-type mechanism (i.e., the fluorine and the terminal oxygen atom of the carbonyl oxide reside in a syn (δ(F−C3−C4−O1)<90°) or an anti (δ(F−C3−C4−O1)>90°) conformation). In the b-type mechanism, the conformations can be defined with respect to the δ(F−C3−O2−O1) dihedral angle in the fluorocarbonyl oxide moiety, according to δ(F−C3−O2−O1) ≈ 0° for a syn and δ(F−C3−O2−O1) ≈ 180° for an anti conformation. All possible routes of cleavage of **POZF** were studied (eight channels in all, please

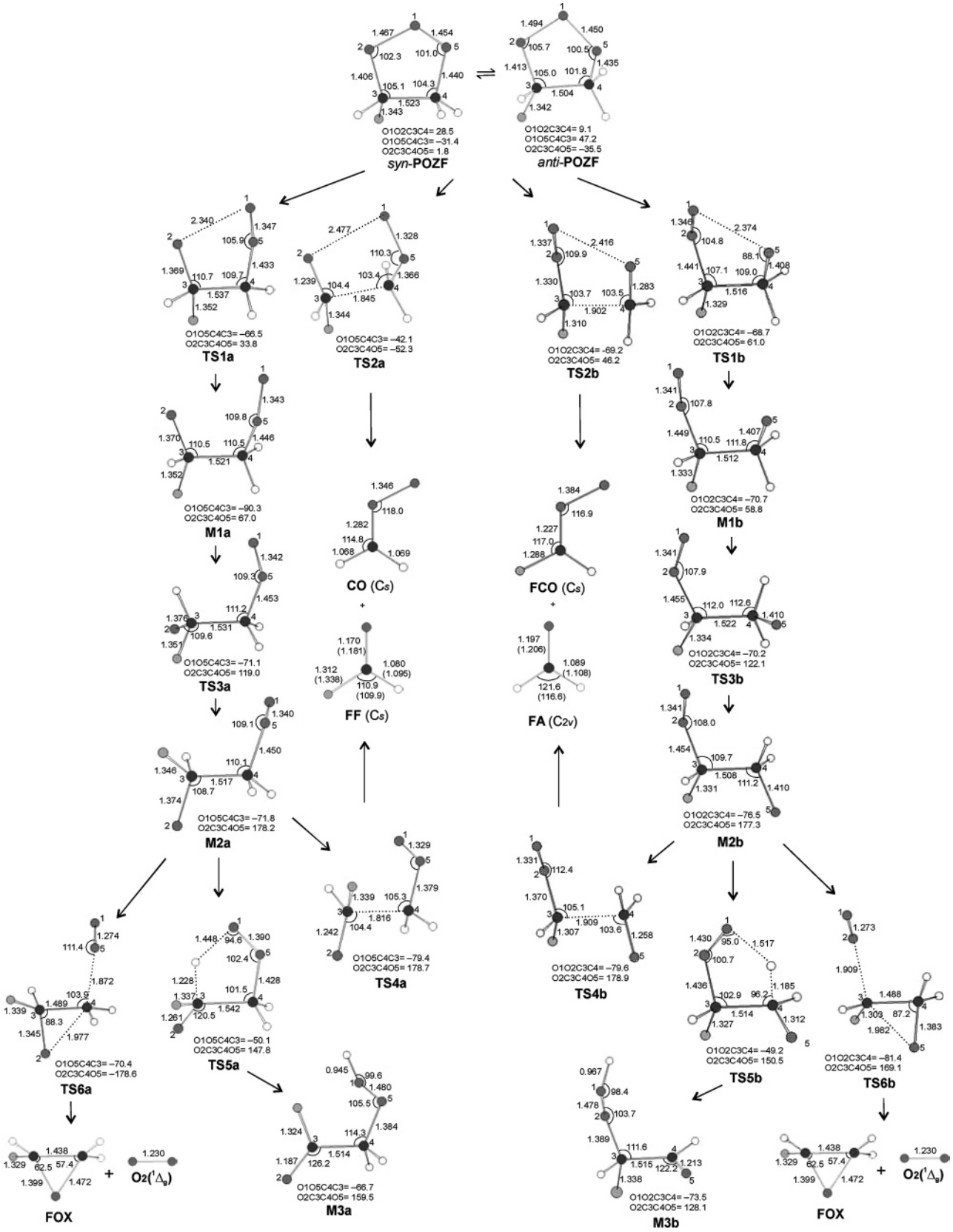

Figure 1. Geometric parameters at the CASSCF(10,9)/cc-pVTZ level (bond lengths in angstroms, angles in degrees) of the species produced in the decomposition of the primary fluorozonide (**POZF**). Experimental data for formyl fluoride (**FF**)[33a] and formaldehyde (**FA**)[33b] are given in parentheses.

see section A below). All of the decomposition channels are accessible regardless of the original conformation of **POZF**, as is discussed in section C. To keep Figure 1 less elaborate, only one conformational isomer of each stationary point is drawn, not necessarily the more stable one, but the differences are generally small (please see section C below). Cartesian coordinates (bohr), CASSCF, CASPT2, and CCSD(T) energies (hartree), and zero-point vibrational energies (kcal mol^{-1}) for all of the stationary points discussed in the paper are available as Supporting Information.

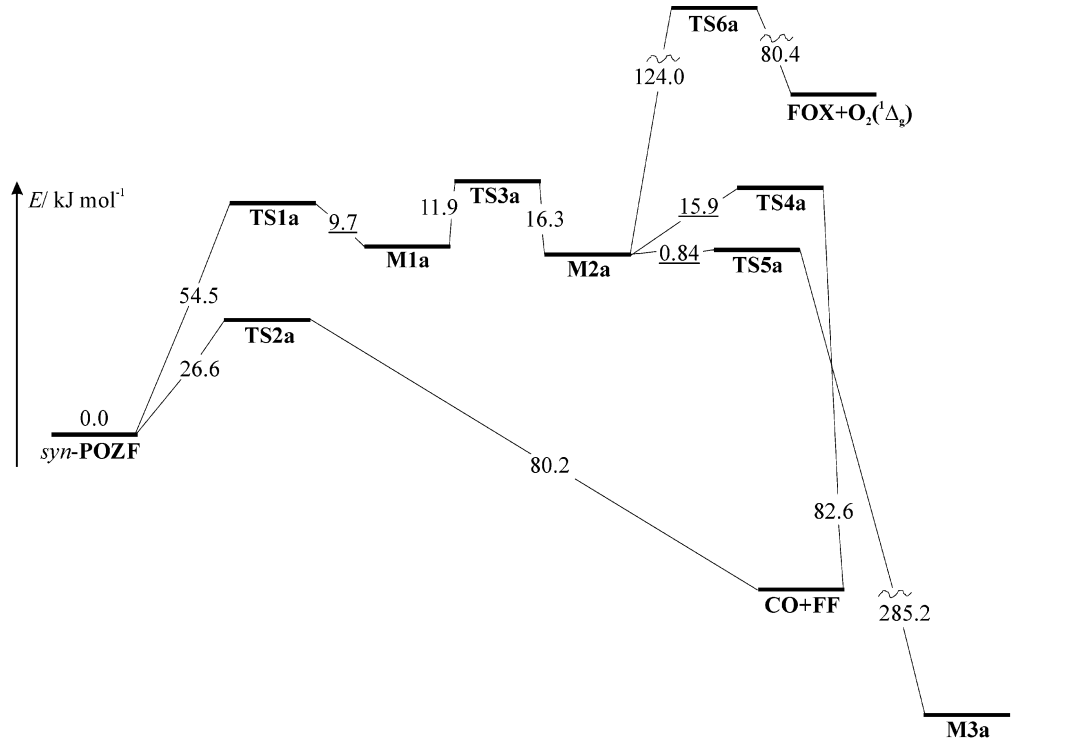

(a)

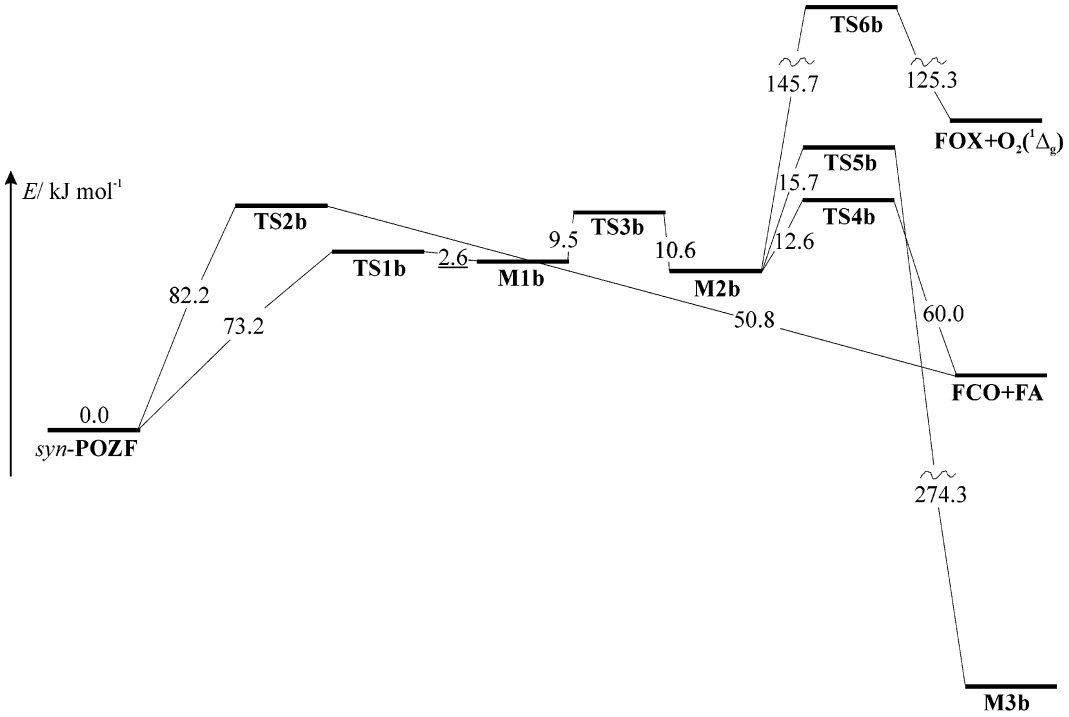

(b)

Figure 2. Reaction profiles for the decomposition of the primary fluorozonide (**POZF**) corresponding to Figure 1 for the (a) a-type mechanism and (b) b-type mechanism at the CASPT2(10,9)/cc-pVTZ level. All relative energies are corrected for the differences in ZPVEs. Underlined relative energies are calculated at the CCSD(T)/6-311G(2d,2p) level.

A. a- versus b-Type Mechanism of the POZF Decomposition. *RRKM Calculations.* As seen from the 1D reaction profiles (Figure 2), the structures from the a-type decomposition are on average 50 kJ mol^{-1} more favorable compared to their b-type counterparts. The difference between the **TS2a** and **TS1b** barriers, which are the two most favorable channels in the a- and b-type decompositions, amounts to 46.6 kJ mol^{-1}. Such a difference in favor of the a-type cleavage, either concerted or stepwise, is expected on the basis of the considerations of geometric trends and relative strengths of the two O−O bonds in both conformational minima of **POZF**, the oxygen envelope (syn) and the H_2C-O half-chair (anti).[17] The predicted principal

TABLE 1: RRKM Rate Constants (s^{-1}) for the POZF Unimolecular Decomposition Channels, Branching Ratios between the a- and b-Type Decompositions ($\Gamma = \sum_{a\ type}k/\sum_{all}k$) and Mean Energies $\langle E\rangle$ (kJ mol^{-1}) of the Chemically Activated POZF over the 145−295 K Temperature Range at 1.013×10^5 Pa Pressure[a]

	k(**TS1a**) $\times 10^{-12}$		k(**TS2a**) $\times 10^{-13}$		k(**TS1b**) $\times 10^{-11}$		k(**TS2b**) $\times 10^{-12}$			
T	syn	anti	syn	anti	syn	anti	syn	anti	Γ	$\langle E\rangle$
145	1.01	1.78	7.14	4.77	2.17	3.04	0.936	1.38	0.977	249.0
175	1.03	1.80	7.26	4.83	2.22	3.11	0.964	1.42	0.977	250.1
205	1.05	1.83	7.40	4.91	2.28	3.20	0.995	1.47	0.977	251.3
235	1.08	1.86	7.54	4.98	2.35	3.30	1.03	1.53	0.976	252.7
265	1.10	1.89	7.70	5.06	2.42	3.40	1.07	1.59	0.976	254.3
295	1.13	1.92	7.86	5.15	2.50	3.51	1.11	1.66	0.975	256.1

[a] The values used for the barriers (kJ mol^{-1}) at 0 K, corrected for the zero-point energies, are as follows: E(*syn*(*anti*)-**TS1a**) = 54.5 (40.5), E(*syn*(*anti*)-**TS2a**) = 29.0 (26.6), E(*syn*(*anti*)-**TS1b**) = 80.0 (73.2), and E(*syn*(*anti*)-**TS2b**) = 87.9 (82.2).

manner of cleavage of **POZF** to H_2COO and HCOF is also in accordance with the experimental findings.[13]

At this point, our aim was to estimate theoretically the branching ratio for the two types of Criegee cleavages using the unimolecular rate constants calculated within the RRKM formalism.[30,31] The calculated constants for the unimolecular decomposition channels and the corresponding branching ratios Γ over a temperature range and at atmospheric pressure ($P = 1.013 \times 10^5$ Pa) are collected in Table 1. In this calculations, all possible manners of unimolecular cleavage of **POZF** are taken into account, specifically syn and anti conformations of the stepwise and concerted transition-state structures **TS1a**(**b**) and **TS2 a**(**b**), which amounts to eight unimolecular channels.

However, as seen from Figure 1, eventually the stepwise mechanisms of the decomposition might not necessarily lead to the Criegee intermediates; in particular, the *a* stepwise mechanism may preferentially lead to hydroperoxyacetyl fluoride (**M3a**, Figures 1 and 2a). Also, biradical intermediates **M1a** and **M1b** resulting from the stepwise decomposition are stabilized only a little with regard to **TS1a** and **TS1b** (Figure 2) so that a kind of equilibrium between **POZF** and these intermediates need be considered. Nonetheless, as is easily verified, other possible ways of calculating the branching ratio, such as taking into account only the concerted decompositions, have a negligible effect on Γ.

The average rate constants at 1.013×10^5 Pa, as well as the **POZF** mean energy, depend only slightly upon the temperature, as is expected for a chemically activated species. The chemical activation by the highly exoergic preceding step produces a very narrow distribution of energies (eq 1), which makes the unimolecular constants rather insensitive to the collision frequency. Therefore, the ratio $\langle k_a\rangle_\infty/\langle k_a\rangle_0$, with subscripts indicating the infinite and zero-pressure limits, is close to unity. It is seen from Table 1 that the mean energy of the chemically activated **POZF** is well above the barriers to all of the decomposition channels, which might point to a breakdown of the strong-collision hypothesis, in particular at lower temperatures and with very small molecules involved in the de-energization by collisions.[31] It was obsevred, however, that the average collision frequency of 3×10^9 s^{-1} at 1.013×10^5 Pa pressure is too low, so the collision stabilization cannot compete to a significant extent with the unimolecular decomposition. Consequently, the model chosen for the de-energization rate, either the strong-collision or stepwise, does not play a major role here. We conclude that the fraction of **POZF** molecules that is stabilized in the observed temperature range must be entirely negligible, in line with similar studies on the chemically activated primary ozonide of ethene.[14i]

Within the RRKM theory, the concerted transition states are generally preferred over the stepwise because of several low-lying vibrational modes that make the densities of states of the concerted transition structures around an order of magnitude larger at a given energy threshold. Thus, for example, the concerted b-type decomposition (**TS2b**) becomes faster than the stepwise (**TS1b**), despite the 9.0 kJ mol^{-1} higher barrier. As is expected, the effect of adiabatic rotations accounted for via the difference in the mean rotational energies (eq 5) contributes to a nonnegligible increase in all of the unimolecular constants, up to 0.3 s^{-1} in the case of **TS2b** at 300 K, whereas the overall effect on the calculated branching ratios is only minor. The calculated branching ratios also exhibit a negligible variation over the observed temperature range. Overall, the mean branching ratio of 0.98 is close to the upper bound of the estimates based on the isotopic labeling experiments at 147 K, according to which 75−95% of **POZF** cleaves according to the a-type mechanism (i.e., preferentially to the H_2COO and HCOF fragments[13]).

In general it was observed that the largest differences are in favor of the a-type structures, which contain a clearly distinguishable moiety of formyl fluoride, as opposed to the formaldehyde moiety from the b mechanism. Thus, the peak difference of 85 kJ mol^{-1} is found between the independent carbonyl oxide-formyl fluoride (**CO-FF)** and fluorocarbonyl oxide-formaldehyde (**FCO-FA)** pairs. Such a marked stability of formyl fluoride, which emerges chiefly at the correlated levels of theory, has long been interpreted as the superposition of the states of the fluorine lone pairs and π density of the carbonyl bond, whereby the fluorine atom acts as a π donor and oxygen acts as a π acceptor.[34] As to the in-plane effects, particularly noteworthy is the anomeric-type delocalization[35] of the O atom lone pairs in an exactly antiperiplanar topology with regard to the σ^*_{C-F} antibonding state. An exceptionally high stabilization due to fluorine substitution on the carbonyl group is also suggested by a large difference of 260 kJ mol^{-1} between experimental enthalpies of formation of formaldehyde and formyl fluoride. For the sake of comparison, upon 1-fluoro substitution the average lowering of the enthalpies of formation of straight-chain hydrocarbons, taken as reference compounds, is about 180 kJ mol^{-1}.

B. Concerted versus Stepwise Decomposition of POZF. The preferred manner of the **POZF** decomposition differs within the a- and b-type mechanisms. From the barrier heights (Table 1 caption), the a type prefers the concerted cleavage by 13.9 kJ mol^{-1}, whereas in the b type the stepwise cleavage is 9.0 kJ mol^{-1} more favorable. Although the RRKM rate constant calculations (vide ante) showed that the concerted decompositions are faster within both mecahnisms, it is nonetheless illustrative to compare the above-mentioned trends from the standpoint of the electronic structure calculations.

In the case of the decomposition of the primary ozonide of ethene (**POZ**),[23] the concerted manner of the **POZ** cleavage is more favorable than the stepwise by 4.2 kJ mol^{-1}, but what

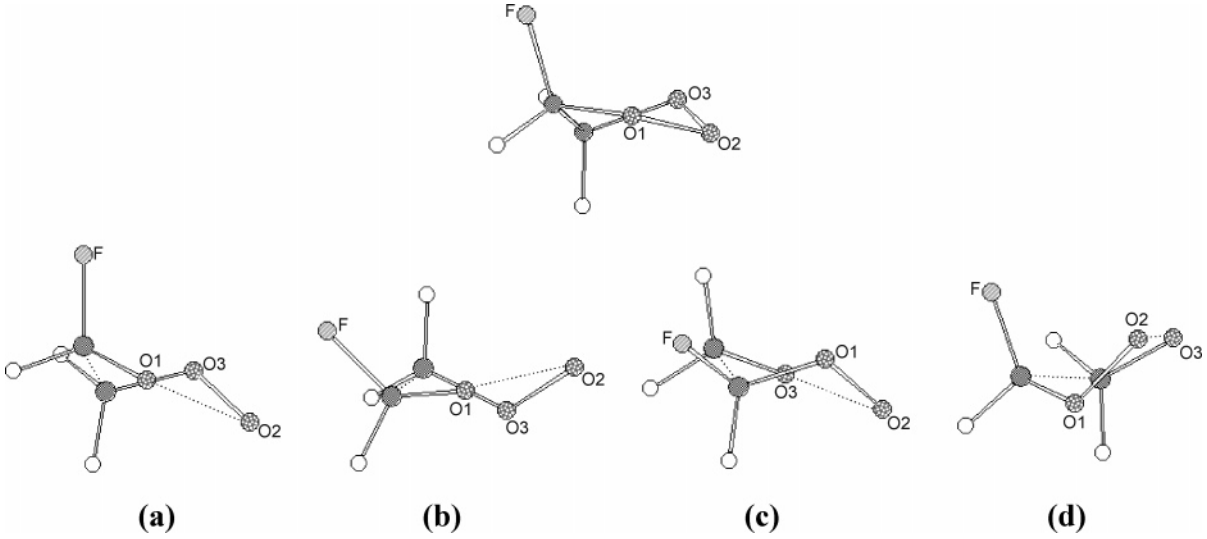

Figure 3. Transition-state structures for the concerted decomposition as derived from the H_2C-O half-chair conformation of **POZF** (top): (a) *anti*-**TS2a**, (b) *syn*-**TS2a**, (c) *anti*-**TS2b**, and (d) *syn*-**TS2b**.

makes it so is only the correction in ZPVE differences between **POZ** and the respective transition-state structures **TS4** and **TS2**, based upon vibrational frequencies calculated at the CASSCF(6,6)/6-31G(d) level. Upon considering the electronic energy difference from this uncorrelated level, one learns that it is strongly, by 115.5 kJ mol^{-1}, in favor of the stepwise mechanism. Upon correcting for the dynamic correlation at the CCSD(T)/6-311G(2d,2p) level, such a huge difference almost vanishes so that the ZPVE correction eventually lowers the barrier to **TS4** beneath that to **TS2**.[23] As to our approach based upon the CASPT2 corrections, this does not change the trends established at the uncorrelated CASSCF/cc-pVTZ level very drastically for the b-type mechanism. Here, despite the ZPVE correction lowering the **TS2b** transition structure by 7.1 kJ mol^{-1} relative to **TS1b**, the stepwise cleavage remains more favorable, which confirms the prediction from the uncorrelated level. However, an interesting thing occurs within the a-type cleavage, where the CASPT2 correction behaves quite similarly to the CCSD(T) correction in the ethene ozonolysis. Thus, the a-type concerted decomposition becomes the preferred one by ~20 kJ mol^{-1}, which is entirely opposite from the uncorrelated CASSCF level, where the stepwise decomposition requires 25 kJ mol^{-1} less activation energy. Similar behavior of CASPT2, in the sense of a marked lowering of the barriers, was observed in the case of a few other transition structures and the processes commonly linked to the emergence of the fluorine-substituted carbonyl group.

C. syn versus anti Conformations of the Stationary Points. With regard to the energy differences between the syn and anti conformations in each of the optimized structures, they are comparably low, which brings about only minor modifications to the calculated relative energies. The relative stability of the conformations can be commonly derived on the basis of general considerations, such as minimizing the repulsion of considerably negatively charged fluorine and the terminal O atom of the carbonyl oxide moiety. When the mutual orientation of these two atoms is opposite, as in the anti conformations, the decrease in repulsion is accompanied by decreased dipole moments, on average by 0.6 and 1.2 D for the a- and b-type structures, respectively.

The interchange of conformations takes place via rotation of the terminal O1 atom around the C4−O5(C3−O2) bonds in a(b) mechanisms. The barriers to interchange calculated for a couple of minima structures (e.g., **M1a**, **M2a**, **M1b**) are quite similar, around 12 kJ mol^{-1} at the CASPT2(10,9)/cc-pVTZ level. These are relatively low because the character of the C4−O5(C3−O2) bond is predominantly single whenever the C1−C2 bond is still not broken. Accordingly, the barriers increase rapidly with the distance between the carbonyl oxide and aldehyde moieties so that at one instance the **FCO** conformation within the b mechanism becomes fixed. The incidence of the cis and trans conformations of **FCO** should be almost equal because the *anti*-**TS2b** and *anti*-**TS4b** structures, whereby the **FCO** fragments emerge directly, are only slightly more stable than their conformational counterparts, *syn*-**TS2b** and *syn*-**TS4b**, by 5.7 kJ mol^{-1} and 0.54 kJ mol^{-1}, respectively (please refer to the Supporting Information). Occasionally, the syn conformations in the b mechanism are more stable, which can be ascribed to the emergence of the stabilizing cis effect in the **FCO** moiety.[36] The trans conformation of **FCO** has additional relevance to atmospheric processes in that it may provide a channel for the OH radical formation through the migration of the H atom to the terminal O atom. It was estimated that this process has nearly 5% probability of occurrence, as opposed to the dominant rearrangement of **FCO** to fluorodioxirane.[36]

Figure 3 renders visible the puckering modes of the 1,2,3-trioxolane ring, which relate the H_2C-O half-chair conformation of **POZF** to the four optimized concerted transition structures.

Attempts to rationalize the stereochemistry of ozonolyses upon the basis of conformational analyses of the transition states for the cycloreversion (**TS2**s) and recurring cycloaddition (**TS7**s) have received considerable attention in the literature.[13,16,37,38] The barriers (kJ mol^{-1}) to the four concerted decompositions are E(*anti*(*syn*)-**TS2a**) = 26.6 (29.0) and E(*anti*(*syn*)-**TS2b**) = 82.2 (87.9). All four concerted transition structures are best described as various stretched half-chairs rather than stretched envelopes. It is seen (Figure 3a) that *anti*-**TS2a** is very easily derived from the H_2C-O half-chair minimum just by elongating the O1−O3 and C−C bonds. A great conformational resemblance between the two structures, with the fluorine atom maintaining a clearly axial site, gives rise to the lowest barrier, in keeping with the Hammond postulate.

In reaching the *syn*-**TS2a** structure (Figure 3b), the H_2C-O half-chair first puckers, whereby the F atom assumes the equatorial site. For this reason, the resulting half-chair is only metastable and cleaves very favorably, which makes for a very small difference between the anti and syn barriers, despite the necessary preliminary puckering movement. All types of

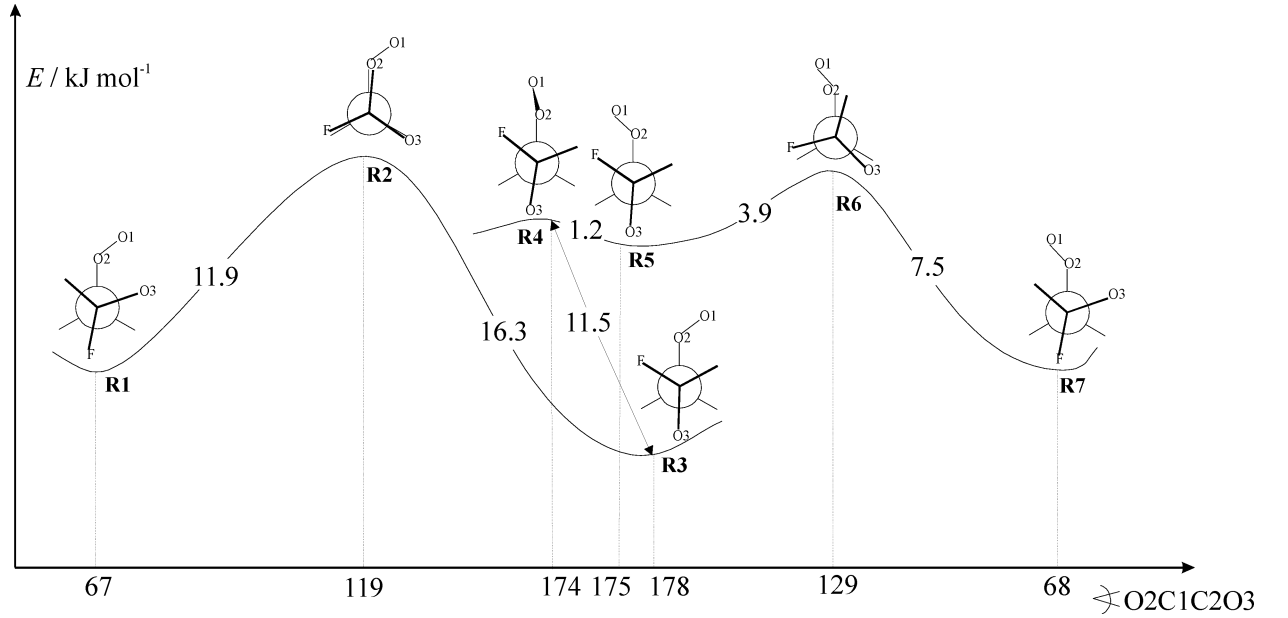

Figure 4. Newman projections along the C−C bond of rotamers from the a-type stepwise decomposition of **POZF** at the CASPT2(10,9)/cc-pVTZ level. All relative energies are corrected for the differences in ZPVEs.

metastable half-chairs, precursors to the **POZF** cleavage, can be observed in the course of the **POZF** optimization if this is initiated from structures closely resembling the concerted transition states. Similar procedures are found to be an excellent alternative to the following reaction path.[17] Here in particular they invariably end up in the H_2C-O half-chair minimum, which confirms that the conformational space of **POZF** contains only two previously described minima.[17] These are governed primarily by maximizing the anomeric stabilization involving the C−F bond and O1 lone pairs.

As to the b mechanism (Figure 3c and d), the conclusion that the formed **FCO** prefers the cis conformation, drawn on the basis of the axial site assumed by the fluorine atom in **POZF**,[11] seems vague. The minor difference in energy in favor of the *anti*-**TS2b** structure, as well as the RRKM calculations, indicate that the incidence of both conformations should be about the same, with the trans conformation being only slightly preferred. Neither transition structure closely resembles the parent **POZF**, with *anti*-**TS2b** being closest to the FHC−O1 half-chair and *syn*-**TS2b** being closest to the O1−O2 half-chair. Within the former, the equatorial position assumed by the F atom enables somewhat easier cleavage and hence the lower barrier to *anti*-**TS2b**. Overall, in case of the fluorine substituent the optimal conformations of the transition states may be difficult to predict, which calls for an increased alert in applying the qualitative schemes for predicting the stereochemistry of ozonolysis.[11,37,38]

D. Decomposition of POZF up to the Formation of the Secondary Fluorozonide. Upon the homolytic rupture of the O1−O2(O1−O5) bond, several rotamers (**R**), minima, and transition states result. Figure 4 shows them depicted in the Newman projection for the a-type stepwise cleavage. The rotamers that are not directly relevant to the overall mechanism were left out of Figure 1. All **R**s are model singlet biradicals, as reflected in their HOMO(LUMO) occupancies, which are very close to 1.0 (e.g., 1.13(0.89) in **R3** (**M2a**)). The 10.3 kJ mol^{-1} rise (Figure 4) in the potential energy, upon rotation of the O1 atom in **R3** (**M2a**) via the **R4** transition structure, can be attributed to the Coulomb repulsive O1−F interactions in the syn conformation **R5**. The accompanying increase in the dipole moment is 0.64 D. It is further seen that **R1** is 2.3 kJ mol^{-1} more stable than **R7**, despite the syn-positioned negatively charged O1 and O3 atoms and 0.89 D larger dipole moment in **R1**. Thus, the attractive interaction between O1 and O3, because these atoms act like radical centers in the rotamers, proves to be more important than their Coulombic repulsion.

Henceforth, the designations for the mechanism (a or b) are left out of the abbreviations for the stationary points whenever the explicit mechanism is not of direct relevance. The nearly equally stable rotamers **M1** and **M2** (Figure 3) are separated by low barriers of approximately 10 kJ mol^{-1}. The key differences between the stepwise and concerted mechanism of the **POZF** cleavage are provided by the two additional routes that **M2** may pursue: (1) rearrangement to peroxyacetyl fluoride in the a-type (**M3a**) or to fluoroperoxyacetaldehyde in the b-type mechanism (**M3b**) via the H atom migrations (**TS5**) or (2) unimolecular decomposition (**TS6**) to the singlet oxygen ($O_2{}^1\Delta_g$) and fluoroxirane (**FOX**). The third path (**TS4**) acts merely as a delayed (two-step) decomposition to the Criegee intermediates.

In **M2**, the apical O1 atom resides in the optimal position to abstract the H atom from the C of the carbonyl subunit. Within both mechanisms, the barriers to **TS5** calculated at the CCSD(T)/6-311G(2d,2p) level turned out to be exceedingly low, only 0.84 kJ mol^{-1} for the a and 15.7 kJ mol^{-1} for the b mechanism. Thus, it can be concluded that **M2** decompose instantaneously, with the H atom abstraction and the delayed decomposition via **TS4** being fully competitive processes. The chemically activated **M2** species are expected to show decreased sensitivity to barrier height so that the difference of 15 kJ mol^{-1} in favor of **TS5a** appears to be irrelevant.

Upon the H atom migration, the **M3** products emerge in markedly exoergic processes. In **M3b**, the C4−O5 carbonyl bond nearly eclipses the hydrogen attached to the vicinal C3, with the δ(O5−C4−C3−H) dihedral angle being 3°. It is well established that double bonds eclipsing hydrogen results in the most stable conformation in many compounds.[8] An unexpected conformation is the one assumed by **M3a**. Here, one does not observe the carbonyl bond favorably eclipsing any of the two hydrogens attached to C4 (δ(O2−C3−C4−H) = 34°(83°) for the two H atoms). Instead, the negatively charged O5 and F atoms curiously assume more of an eclipsed than a gauche

position (δ(F−C3−C4−O5) ≈ 23°). The occurrence is similar to the gauche effect studied chiefly in connection to the rotamers of 1,2-difluoroethane.[39] However, in **M3a** the double carbonyl bond vicinal to the fluorine makes for a structural peculiarity that places the observed trend in the F−C3−C4−O5 dihedral angle halfway between the gauche and cis effects. The extent to which the two highly electronegative atoms are eclipsed correlates well with the electron density in the C3−C4 region, a result that may perhaps be generalized.[36]

Naturally, the highly energized **M3a** and **M3b** species may undergo various further bond fisions, of which the O−O bond fission appears to be particularly interesting because it may provide an additional channel for OH radical production in gas-phase ozonolyses. In the ozonolysis of ethene, such a channel seems likely because the pair of resulting radical species was shown to be more stable than the primary ozonide.[23]

Although the remaining decomposition channels of **M2a**(**M2b**) yielding **FOX** and $O_2(^1\Delta_g)$ via **TS6a**(**TS6b**) are 35(13 kJ mol^{-1}) more favorable than the analogous process in the ozonolysis of ethene,[23] their overall role appears to be negligible compared to that of the two dominant processes discussed above. Mazur et al.[11,13] in particular emphasize that not even traces of **FOX** were observed in the experiment, although in fact the direct epoxidation of fluoroethene by **FCO** in the reaction mixture is the principal process whereby **FOX** might have been expected.[12]

E. CASPT2 versus CCSD(T) Correction. Modeling of the first addition step and kinetic parameters of the ethene, fluoroethene, and chloroethene ozonolyses showed that the CASSCF/CASPT2 approach is capable of yielding results that compare very well with the experiment.[17] This encouraged further use of this simple approach in describing the intricate routes of the unimolecular decomposition of **POZF**. However, within some decomposition channels difficulties arose in that the multireference PT2 correction lowered the energy of the transition structure to the extent of placing it below that of the preceding minimum, which made the corresponding barrier negative and thus unphysical. As a rule, all of these transition structures are of a very early type connecting biradical shallow minima with the "exoergic abysses", which are in turn commonly linked to the emergence of the fluorine-substituted carbonyl group (Figures 2 and 7). Whenever this occurred, the CASPT2 corrections were substituted by the CCSD(T) corrections based on the restricted HF reference and the 6-311G(2d,2p) basis set. This basis set, which is probably near the smallest allowed in the context of sensible coupled cluster calculations,[40] was actually the largest possible that we could use in present studies on a system of this size.

In an attempt to elucidate the poor performance of CASPT2 and to obtain a more reasonable CASPT2 estimate of the barriers in question, we decided to investigate the case of **TS4a** in more detail. At this point, the CASSCF optimization of **M2a** was performed, which had been initiated from a geometry very similar to that of **TS4a**. In the course of the optimization, around 10 new geometries were generated resting along a quasi-CASSCF minimum-energy path, and in each of these geometries, the CASPT2 correction was calculated. The obtained CASPT2 energies varied significantly with small changes in the C−C distance, as a consequence of significant changes in the active occupancies. It was concluded that the CASSCF C−C distance of 1.816 Å in **TS4a** already well exceeds what would be the transition C−C distance on the CASPT2 potential surface. Consequently, from the CASPT2 standpoint, the CASSCF **TS4a** structure is positioned well along the descent toward the **CO-FF** minimum. Thus, the negative barrier is not a shortcoming of the CASPT2 approach, but rather the CASPT2 saddle point is shifted toward shorter C−C distances, with our best estimate in the vicinity of 1.68 Å. With still shorter C−C distances, the CASPT2 corrections exhibit a monotonic drop toward the biradical **M2a** minimum. When the barrier is reevaluated using the highest observed CASPT2 energy (d(C−C) = 1.676 Å), it now equals 5 kJ mol^{-1}. There are indications that this value is much closer to the CCSD(T) infinite basis limit than is the CCSD(T)/6-311G(2d,2p) result.

We further tested various active spaces, ranging from minimal (2,2) to (14,13), at the very edge of what is presently possible. In all of these calculations, the negative barrier persisted. Thus, it was concluded that whenever the CASPT2 correction to the CASSCF stationary geometries resulted in negative barriers these were not due to imbalances in the (10,9) active space but rather were due to discrepancies between the CASSCF and CASPT2 potential surfaces as to the position of the stationary structures. Overall, within the CASSCF/CASPT2 approach such occurrences are associated with what would indeed be low barriers (<10 kJ mol^{-1}) and hence can be an indication of almost instantaneous processes.

Although the CCSD(T) corrections evaluated at the CASSCF optimized geometries resulted in positive barriers, which could be substituted for the CASPT2 barriers in the reaction profiles, we believe that there is no particular need to favor the CCSD(T) correction over the CASPT2 in all cases. The problem with the CCSD(T) arises in connection to the RHF function used for the clearly biradical minima, which are followed by the transition states that are significantly less biradical in character. Better insight into the extent of near-degeneracy effects is provided by the T_1 diagnostic,[28] which proved to be quite large, close to 0.04 in **M2a** and **M4** (discussed below), but somewhat less, 0.02−0.03 in the **TS4a**, **TS5a**, **TS11**, and **TS13** transition structures (please see the Supporting Information). It is known that T_1 values larger than 0.02 indicate a greater importance of nondynamical correlation and thus an increasing unreliability of the RHF reference.[40] In such situations, correcting for connected triples proves to be of vital importance. In particular, good agreement between the CC methods that correct for connected triples and MCSCF/MRCI approaches was seen in systems where T_1 was as large as 0.04.[40] Because similar large values of T_1 are inherent to singlet biradical species such as **M4**, a noniterative account of the triples, as in CCSD(T), might yield reliable enough energy differences.

F. Secondary Fluorozonide. Upon cycloreversion of **POZF** and mutual rotation of the resulting Criegee fragments, the two can reunite in yet another 1,3-bipolar addition to form the secondary fluorozonide (**SOZF**). The described sequence of events is relevant primarily for the condensed phase.[7] In the case of ethene ozonolysis, Cremer et al.[14f] suggested that the change in orientation of the fragments takes place via a rigid dipole vdW complex confined within the solvent cage, which was accepted by other authors as a general modification of the ozonolytic mechanism.[14h] These complexes seem capable of guiding the fragments stereospecifically (in the case of 1,2 disubstituted ethenes) toward the secondary ozonides while at the same time providing an explanation for the lack of spectroscopic verification of carbonyl oxides under conditions of ozonolyses.[15] At the CASSCF(10,9)/cc-pVTZ level, we managed to find only approximate structures of the complexes formed by the **FCO-FA** and **CO-FF** fragment pairs. Preliminary CC calculations show that a considerable dipole stabilization may be expected, but because the corresponding stationary points are not confirmed, they are omitted from the mechanism.

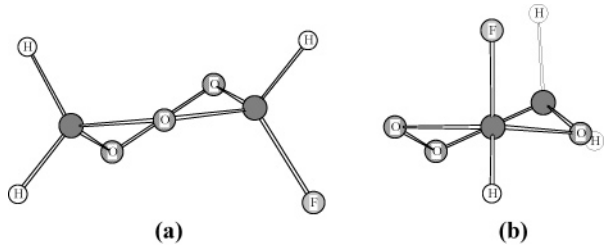

Figure 5. Two basic conformations of the 1,2,4-trioxolane ring of the secondary fluorozonide: (a) O−O half-chair and (b) H_2C−O half-chair.

We found two distinctive conformational minima of **SOZF**, designated **SOZFa** and **SOZFb**, as results of the optimizations initiated from the *syn*- and *anti*-**TS8** geometries, which were only slightly perturbed in the direction of the products. Such procedures are completely analogous to those carried out in the optimization of **POZF**[17] and are valuable in retaining the analogous structures of the active spaces, which proves essential for a sensible comparison of the multireference-based energies. The resulting two conformational minima of **SFOZ** are depicted in Figure 5. The predicted more-stable conformation (**SOZFa**, Figure 5a) is a twisted O−O (peroxy bridge) half-chair, found also in several other secondary ozonides,[38] with the fluorine atom occupying the axial site. This conformation is also in accordance with the experimental assignments of the MW spectra.[11] The 8.0 kJ mol^{-1} less stable conformation (**SOZFb**, Figure 5b) is best described as a H_2C−O half-chair.

The rotational constants (MHz), derived from the CASSCF-(10,9)/cc-pVTZ optimized geometry, are comparable to the experimental constants[11] given in parentheses: 6813 (6774), 3988 (3916), 3155 (3123). Upon applying the well-established scaling factor of 0.89 for the CASSCF wavenumbers, these, together with the predicted intensities, are also found to correlate well with the experimental IR spectrum,[11] as seen in Table 2.

The anomeric stabilization[35] in **SOZF** results primarily from combining the near-lying states of the antibonding C−F interaction (σ^*_{C-F}) and the lone pairs of the sp^3-hybridized O atom of the ether bridge. The effect plays a key role in governing the geometric trends in the two conformational minima of **SOZF** in a way similar to that demonstrated for **POZF**.[17] A qualitative analysis of the anomeric effect, analogous to the one carried out in case of the primary fluorozonides,[17] showed that the orientation of the O atom lone pairs with regard to the C−F bond is nearly antiperiplanar (170°) in the O−O half-chair and somewhat more staggered (160°) in the H_2C−O half-chair.

G. Decomposition of the Secondary Fluorozonide. The CASSCF/cc-pVTZ optimized structures of minima and transition states involved in the production and decomposition of **SOZF** are given in Figure 6. The corresponding potential energy profile is given in Figure 7. The profile is given in terms of the relative electronic energies corrected for the diferences in ZPVEs. Two of these are underlined because again the corresponding CASPT2 barriers had to be substituted by the CCSD(T)/6-311G(2d,2p) corrections.

By analogy to the decomposition of **POZF**, the secondary fluorozonide (**SOZF**) may decompose in either a concerted or stepwise manner via transition structures **TS8** and **TS9**, respectively (Figures 6 and 7). It is seen, however, that the cycloreversion via **TS7** is equally competitive. The **TS8** and **TS9** channels include the rupture of the peroxide bridge, the viability of which is indicated by the presence of the O−O bonding and antibonding interaction in the **SOZF** active space, with occupancies of 1.936 and 0.067, respectively. The simultaneous presence of the C2−O1 and C4−O5 bonding and antibonding interactions (1.973−0.028) prompted us to test yet another manner of concerted decomposition of **SOZF**, the one leading to **FOX** and $O_2(^1\Delta_g)$ at this instant. However, because of the high CASPT2 barrier of 445 kJ mol^{-1} (Figure 7) to the transition structure **TS10**, such a decomposition is entirely noncompetitive.

The concerted decomposition of **SOZF** is 29.6 kJ mol^{-1} less favorable than the stepwise decomposition leading to the products fluorodioxirane (**FDOX**) and formaldehide (**FA**) in a single step. The biradical open-ring form of **FDOX**, fluorodioxymethane, is much less stable than **FDOX** owing to the presence of the fluorine substituent.[36] Consequently, the fluorodioxymethane-**FA** pair is actually higher in energy than **TS8** so that **TS8** is directly connected to the **FDOX-FA** pair in Figure 7 without considering the intermediate open-ring form. Likewise, the geometrical trends as well as the active orbitals in **TS8** do not prefer fluorodioxymethane as opposed to **FDOX** because the distance between O1 and O3 of 2.29 Å in **TS8** is actually very similar to the O−O distance in the very early transition state connecting fluorodioxymethane to **FDOX** (2.27 Å).[36] The IRC calculation gives further support to the conclusion that **TS8** leads to **FDOX** directly, and the same conclusion is reached for the **TS12** case (vide infra). Subsequent unimolecular decomposition channels of **FDOX** have been thoroughly investigated recently.[36] It is of interest that an analogous possibility of a concerted decomposition of the secondary ozonide of ethene (**SOZ**) was not found. Anglada et al.[23] concluded that such a channel would be unlikely because the π bonds are not simultaneously formed during the separation of the fragments dioxirane and formaldehide, which is in contrast to the situtation with the concerted decomposition of the primary ozonide. Because in this respect there appears to be no significant difference between **SOZ** and **SOZF**, the reason for the existence of a quite competitive concerted-type decompostion in the case of **SOZF** may lie in the difference in strengths

TABLE 2: Calculated (CASSCF(10,9)/cc-pVTZ, Scaling Factor = 0.89) and Experimental Harmonic Wavenumbers[11] (cm^{-1}), Intensities (km mol^{-1}), and Approximate Assignment of Modes for the O−O Half-Chair Conformation of the Fluoroethene Secondary Ozonide (SOZFa)

CASSCF(10,9)/cc-pVTZ			experimental	
wavenumbers	intensities	assignment	wavenumbers	intensities
1004	40	ring stretch	1005	medium
1079	109	C4−H_2 rock + C2−F stretch	1050	strong
1102	97	C4−H_2 rock	1078	strong
1139	353	C2−O3−C4 ring stretch	1112	very strong
1292	21	C2−H wag + C4−H_2 wag	1300	very weak
1353	36	C2−H wag	1350	weak
1382	36	C4−H_2 wag	1390	weak
2936	22	C4−H_2 asymm. stretch	2910	weak
2946	26	C2−H stretch	3010	very weak

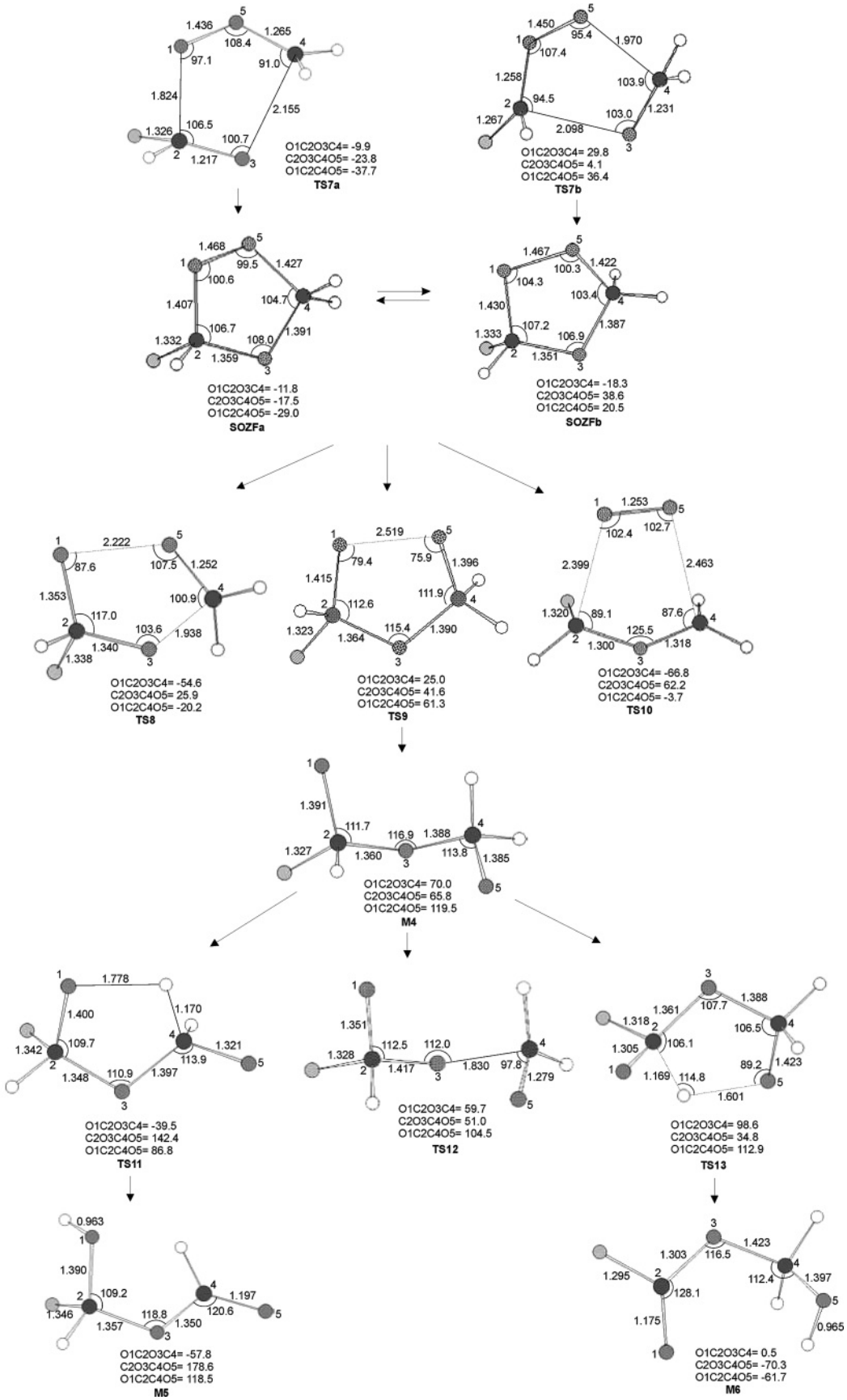

Figure 6. Geometric parameters at the CASSCF(10,9)/cc-pVTZ level (bond lengths in angstroms, angles in degrees) of the species involved in the production and decomposition of the secondary fluorozonide (**SOZF**).

of the C−O bonds of the ether bridge, where the C4−O3 bond is notably more elongated and weaker. It was generally found that halogen substituents, chiefly because of their electronegativity, shorten and strengthen the vicinal bonds but elongate and weaken those next to vicinal,[41] which can also be deduced from the geometric trends in **POZF** and **SOZF**. In connection to this,

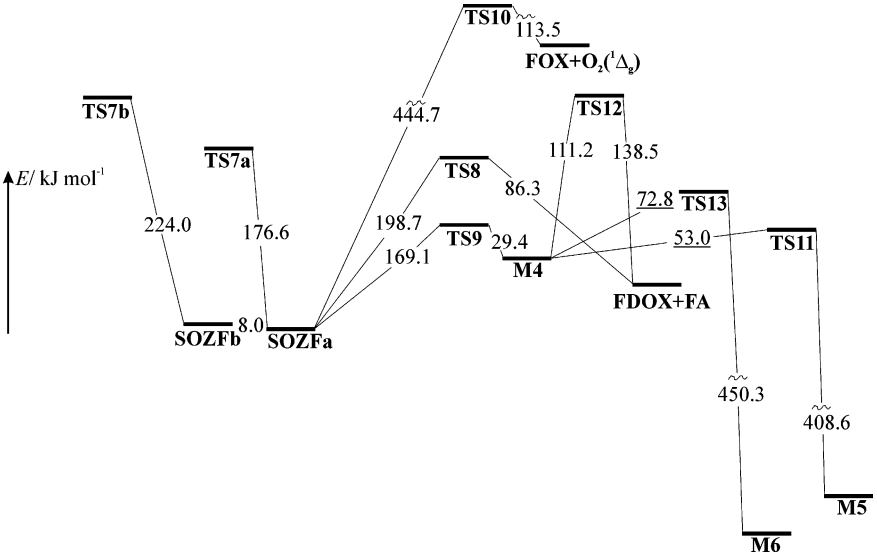

Figure 7. Reaction profile for the production and decomposition of the secondary fluorozonide (**SOZF**) at the CASPT2(10,9)/cc-pVTZ level. All relative energies are corrected for the differences in ZPVEs. Underlined relative energies are calculated at the CCSD(T)/6-311G(2d,2p) level.

we stress that no possibility was found for a concerted decompositon of **SOZF** to dioxirane and formyl fluoride.

The stepwise decomposition of **SOZF** via **TS9** results in a singlet biradical intermediate **M4**, with HOMO−LUMO occupancies of 1.030−0.972. This may subsequently lead to three diferent decomposition routes: (1) the decomposition to **FDOX** and **FA** via **TS12** and (2) and (3) two different H abstractions, either by the O1 or O5 atom via the transition structure **TS11** or **TS13** (Figure 6). Channel 1 is seen to be only slightly competitive (Figure 7) because it does not include the formation of a highly stabilizing species such as formyl fluoride.

However, abstractions 2 and 3 are very competitive processes. (The barrier to the H migration on O1 is 20 kJ mol^{-1} more favorable.) The corresponding barriers had to be substituted by the CCSD(T)/6-311G(2d,2p) method, although they remain of questionable reliability given that the biradical character is clearly expressed in **M4** but only partially so in **TS11** (1.380−0.622) and **TS13** (1.538−0.468). The exaggerated lowering of barriers by the CASPT2 method in analogous situations was stressed several times and discussed earlier in the paper. Here, however, the CASPT2 correction results in only minimally negative barriers, which again might indicate that the two H migrations are almost barrierless processes taking place over exoergic abysses. At the bottom of these abysses lie the two fairly conventional products, hydroxyfluoromethyl formate (**M5**) and hydroxymethyl fluoroformate (**M6**), bearing nothing of the biradical character of their precursors. Interestingly, in **M5** and **M6** the (H, C4, O5, O3, C2) and (F, C2, O1, O3, C4) sets of atoms are almost coplanar. Because of the presence of the fluoro-substituted carbonyl subunit, **M6** proved more stable than **M5**, although only by 22 kJ mol^{-1}, which is probably due to an additional stabilization in **M5** via H−F hydrogen bonding. The corresponding H−F distance in **M5** is very small (1.74 Å), which indicates that **M5** might easily undergo further decomposition to formic acid anhydride and hydrogen fluoride.

Conclusions

Upon the 1,3-bipolar addition of ozone to fluoroethene, the primary fluorozonide (**POZF**) is formed as a short-lived energized species, which undergoes a rapid decomposition. The decomposition takes place in either a concerted or stepwise manner. Within the former, in a single step, any of the two pairs of Criegee intermediates may result, carbonyl oxide (CO) and formyl fluoride (FF) or fluorocarbonyl oxide (FCO) and formaldehyde (FA). The average branching ratio over a temperature range calculated from the RRKM unimolecular rate constants equals 0.98 in favor of the decomposition to CO and FF, which is close to the upper bound of the experimental estimates in the range of 75−95%.[13]

Within the stepwise manner, a biradical intermediate occurs, which acts as a precursor to two more distinctive reaction routes: hydrogen migration to the terminal oxygen atom as well as elimination of the singlet oxygen accompanied by the production of fluoroepoxide. From the barrier heights to these processes, one infers that in particular the hydrogen abstraction is competitive.

In the condensed phase, the Criegee intermediates can reunite in yet another 1,3-bipolar addition to form the secondary fluorozonide (**SOZF**). The two basic conformational minima of **SOZF** are the O−O half-chair and the H_2C−O half-chair. In both conformations, the fluorine atom prefers a clearly axial position with regard to the 1,2,4-trioxolane ring. The scaled calculated wavenumbers and intensities for the half-chair conformation agree well with the O−O (peroxy bridge) twisted half-chair experimental wavenumbers and assignments. By analogy to **POZF**, anomeric stabilization involving the oxygen lone pairs and the C−F bond governs the geometric trends and conformational minima of **SOZF**.

The decomposition of **SOZF** may take place in a stepwise or concerted manner, both of which include rupture of the peroxide bridge. Equally competitive is the cycloreversion to the Criegee intermediates. The most favorable of the routes, the stepwise cleavage of the O−O bond, results in a biradical intermediate that may subsequently pursue two different H migrations to yield hydroxyfluoromethyl formate or hydroxymethyl fluoroformate. These compounds are produced in markedly exoergic processes and so are prone to further decomposition.

Acknowledgment. This work was supported by the Ministry of Science and Technology of the Republic of Croatia under project number 0098033.

Supporting Information Available: Cartesian coordinates (bohr) and CASSCF, CASPT2, and CCSD(T) energies (hartree) for the stationary points discussed in the paper. This material is available free of charge via the Internet at http://pubs.acs.org.

References and Notes

(1) Atkinson, R.; Carter, W. P. L. *Chem. Rev.* **1984**, *84*, 437.

(2) Atkinson, R. Gas-Phase Tropospheric Chemistry of Organic Compounds. *J. Phys. Chem. Ref. Data*; American Institute of Physics: New York, 1994; Monograph No. 2.

(3) Finlayson-Pitts, B. J.; Pitts, J. N., Jr. *Chemistry of the Upper and Lower Atmosphere: Theory, Experiments, and Applications*; Academic Press: San Diego, CA, 2000.

(4) IARC: *Some Chemicals Used in Plastics and Elastomers. Vinyl Fluoride*; IARC Monographs on the Evaluation of Carcinogenic Risk of Chemicals to Humans; IARC: Lyon, France, 1986; Vol. 39, pp 147−154.

(5) EPA. U.S. Environmental Protection Agency. Vinyl Fluoride (CAS no. 75-02-5). Office of Pollution Prevention and Toxics; http://www.epa.gov/oppt/chemtest/fluora.pdf; 1990.

(6) Cantoreggi, S.; Keller, D. A. *Toxicol. Appl. Pharmacol.* **1997**, *143*, 130.

(7) Bailey, P. S. *Ozonization in Organic Chemistry*; Academic Press: New York, 1978; Vol. 1.

(8) Hendrickson, J. B.; Cram, D. J.; Hammond, G. S. *Organic Chemistry*, 3rd ed.; McGraw-Hill: Tokyo, 1970.

(9) Criegee, R. *Angew. Chem., Int. Ed. Engl.* **1975**, *14*, 745.

(10) (a) Fenske, J. D.; Hasson, A. S.; Paulson, S. E.; Kuwata, K. T.; Ho, A.; Houk, K. N. *J. Phys. Chem. A* **2000**, *104*, 7821 and references therein. (b) Clark R. J. H.; Foley L. J. *J. Phys. Chem. A* **2002**, *106*, 3356.

(11) Mazur, U.; Lattimer, R. P.; Lopata, A.; Kuczkowski, R. L. *J. Org. Chem.* **1979**, *44*, 3181.

(12) (a) Agopovich, J. W.; Gillies, C. W. *J. Am. Chem. Soc.* **1982**, *104*, 813. (b) Agopovich, J. W.; Gillies, C. W. *J. Am. Chem. Soc.* **1983**, *105*, 5047.

(13) Mazur, U.; Kuczkowski, R. L. *J. Org. Chem.* **1979**, *44*, 3185.

(14) (a) Harding, L. B.; Goddard, W. A., III. *J. Am. Chem. Soc.* **1978**, *100*, 7180. (b) Cremer, D. *J. Chem. Phys.* **1979**, *70*, 1898. (c) Cremer, D. *J. Am. Chem. Soc.* **1981**, *103*, 3619. (d) Cremer, D. *J. Am. Chem. Soc.* **1981**, *103*, 3627. (e) Dewar, M. J. S.; Hwang, J. C.; Kuhn, D. R. *J. Am. Chem. Soc.* **1991**, *113*, 735. (f) Cremer, D.; Kraka, E.; McKee, M. L.; Radhakrishnan, T. P. *Chem. Phys. Lett.* **1991**, *187*, 491. (g) Cremer, D.; Gauss, J.; Kraka, E.; Stanton, J. F.; Bartlett, R. *Chem. Phys. Lett.* **1993**, *209*, 547. (h) Ponec, R.; Yuzhakov, G.; Haas, Y.; Samuni, U. *J. Org. Chem.* **1997**, *62*, 2757. (i) Olzmann, M.; Kraka, E.; Cremer, D.; Gutbrod, R.; Andersson, S. *J. Phys. Chem. A* **1997**, *101*, 9421.

(15) Bunnelle, W. H. *Chem. Rev.* **1991**, *91*, 335.

(16) Cremer, D. *J. Am. Chem. Soc.* **1981**, *103*, 3633.

(17) Ljubić, I.; Sabljić, A. *J. Phys. Chem. A* **2002**, *106*, 4745.

(18) Roos, B. O.; Taylor, P. R.; Siegbahn, P. E. M. *Chem. Phys.* **1980**, *48*, 157.

(19) Andersson, K.; Malmqvist, P.-Å; Roos, B. O. *J. Chem. Phys.* **1992**, *96*, 1218.

(20) Borowski, P.; Andersson, K.; Malmqvist, P.-Å; Roos, B. O. *J. Chem. Phys.* **1992**, *97*, 5568.

(21) Ljubić, I.; Sabljić, A. *Chem. Phys. Lett.* **2004**, *385*, 214.

(22) Chen, B.-Z.; Anglada, J. M.; Huang, M.-B.; Kong, F. *J. Phys. Chem. A* **2002**, *106*, 1877.

(23) Anglada, J. M.; Crehuet, R.; Bofill, J. M. *Chem.—Eur. J.* **1999**, *5*, 1809.

(24) (a) Dunning, T. H., Jr. *J. Chem. Phys.* **1989**, *90*, 1007. (b) Woon, D. E.; Dunning, T. H., Jr. *J. Chem. Phys.* **1993**, *98*, 1358.

(25) Anglada, J. M.; Bofill, J. M. *Chem. Phys. Lett.* **1995**, *243*, 151.

(26) Raghavachari, K.; Trucks, G. W.; Pople, J. A.; Head-Gordon, M. *Chem. Phys. Lett.* **1989**, *157*, 479.

(27) (a) Krishnan, R.; Binkley, J. S.; Seeger, R.; Pople, J. A. *J. Chem. Phys.* **1980**, *72*, 650. (b) McLean, A. D.; Chandler, G. S. *J. Chem. Phys.* **1980**, *72*, 5639.

(28) Lee, T. J.; Taylor, P. R. *Int. J. Quantum Chem. Symp.* **1989**, *23*, 199.

(29) Andersson, K.; Barysz, M.; Berndhardsson, A.; Blomberg, M. R. A.; Cooper, D. L.; Fleig, T.; Fülscher, M. P.; de Graaf, C.; Hess, B. A.; Karlström, G.; Lindh, R.; Malmqvist, P.-Å.; Neogrády, P.; Olsen, J.; Roos, B. O.; Sadlej, A. J.; Schütz, M.; Schimmelpfennig, B.; Seijo, L.; Serrano-Andres, L.; Siegbahn, P. E. M.; Stårling, J.; Thorsteinsson, T.; Veryazov, V.; Widmark, P.-O. *MOLCAS*, version 5.4; Lund University: Sweden, 2000.

(30) Marcus, R. A. *J. Chem. Phys.* **1952**, *20*, 359.

(31) Robinson, P. J.; Holbrook, K. A. *Unimolecular Reactions*; Wiley: New York, 1972.

(32) (a) Beyer, T.; Swinehart, D. F. *Comm. Assoz. Comput. Mach.* **1973**, *16*, 379. (b) Stein, S. E.; Rabinovitch, B. S. *J. Chem. Phys.* **1973**, *58*, 2438.

(33) (a) Miller, R. F.; Curl, R. F. *J. Chem. Phys.* **1961**, *34*, 1847. (b) Takagi, K.; Oka, T. *J. Phys. Soc. Jpn.* **1963**, *18*, 1174.

(34) Radom, L.; Hehre, W. J.; Pople, J. A. *J. Am. Chem. Soc.* **1971**, *93*, 289.

(35) Schleyer, P. v. R.; Kos, A. J. *Tetrahedron* **1983**, *39*, 1141.

(36) Ljubić, I.; Sabljić, A. *Chem. Phys*. **2005**, *309*, 157.

(37) Bauld, N. L.; Thompson, J. A.; Hudson, C. E.; Bailey, P. S. *J. Am. Chem. Soc.* **1968**, *90*, 1822.

(38) Lattimer, R. P.; Kuczkowski, R. L.; Gillies, C. W. *J. Am. Chem. Soc.* **1974**, *96*, 348.

(39) Engkvist, O.; Karlström, G.; Widmark, P.-O. *Chem. Phys. Lett.* **1997**, *265*, 19.

(40) Taylor, P. In *Lecture Notes in Quantum Chemistry II*; Roos, B. O., Ed.; Springer-Verlag: Berlin, 1994.

(41) Hu, H.; Gong, M.; Tian, A.; Wong, N. *Int. J. Quantum Chem.* **2003**, *91*, 675.